



Pitchfork–Hopf bifurcations in 1D neural field models with transmission delays



K. Dijkstra^{a,*}, S.A. van Gils^{a,b}, S.G. Janssens^b, Yu.A. Kuznetsov^{b,a}, S. Visser^c

^a Department of Applied Mathematics, University of Twente, P.O. Box 217, 7500 AE, Enschede, The Netherlands

^b Department of Mathematics, Utrecht University, Budapestlaan 6, 3584CD Utrecht, The Netherlands

^c Department of Mathematics, Nottingham University, Lenton Lane, NG7 2NR Nottingham, United Kingdom

HIGHLIGHTS

- We study bifurcations in neural field equations with transmission delays.
- We focus on symmetry to give an efficient method for spectral computations.
- Using residue calculus we show how normal form coefficients can be evaluated.
- To illustrate the methods mentioned above we extensively study two particular pitchfork–Hopf bifurcations.

ARTICLE INFO

Article history:

Received 13 December 2013

Received in revised form

17 June 2014

Accepted 19 January 2015

Available online 28 January 2015

Communicated by S. Coombes

Keywords:

Neural field

Delay equation

Normal form

Numerical bifurcation analysis

Pitchfork–Hopf bifurcation

ABSTRACT

Recently, local bifurcation theory for delayed neural fields was developed. In this paper, we show how symmetry arguments and residue calculus can be used to simplify the computation of the spectrum in special cases and the evaluation of the normal form coefficients, respectively. This is done hand in hand with an extensive study of two pitchfork–Hopf bifurcations for a 1D neural field model with ‘Wizard hat’ type connectivity.

© 2015 Elsevier B.V. All rights reserved.

1. Introduction

The most natural computational models of the brain are networks of spiking neurons. Models of individual neurons in such networks range from very detailed, biophysically realistic multi-compartment models (e.g. [1,2]) to purely phenomenological spiking models (e.g. [3–5]). The drawback of these network models is that the very high dimensionality of parameter and state space makes them analytically intractable and inefficient for numerical simulations. Moreover, large network simulations provide little insight into global dynamical properties. The human brain contains roughly 100 billion (10^{11}) neurons, each forming thousands of connections [6]. As a result, the number of neurons and synapses in

even a very small patch of brain tissue is immense. Therefore, a popular approach to circumvent the problems mentioned above is to take the continuum limit of a neural network in which individual spikes are replaced by a spiking rate and space is continuous. These so-called neural field models are based on the seminal work of Wilson and Cowan [7,8], Amari [9,10] and Nunez [11] in the 1970s and are formulated as nonlinear integro-differential equations. One modification of these original models which has received considerable attention is the incorporation of delays [12–19]. Delays in neural networks arise due to the finite propagation velocities of action potentials along the axons, synaptic processing and dendritic integration [20].

In this paper, we examine the evolution of a single population of neurons that occupy fixed positions in a bounded and open domain $\Omega \subset \mathbb{R}^n$. Let $V(t, \mathbf{r})$ be the averaged pre-synaptic membrane potential at time t of neurons at position $\mathbf{r} \in \Omega$. In the absence of external stimuli, this potential is hypothesized to evolve according

* Corresponding author.

E-mail address: k.dijkstra-1@utwente.nl (K. Dijkstra).

to the integro-differential equation

$$\frac{\partial V}{\partial t}(t, \mathbf{r}) = -\alpha V(t, \mathbf{r}) + \int_{\Omega} J(\mathbf{r}, \mathbf{r}') S(V(t - \tau(\mathbf{r}, \mathbf{r}'), \mathbf{r}')) d\mathbf{r}'. \quad (\text{NFE})$$

The intrinsic dynamics are given by exponential decay with rate $\alpha > 0$. The propagation delay $\tau \in C(\bar{\Omega} \times \bar{\Omega})$ measures the time it takes for a signal sent by a neuron located at position \mathbf{r}' to reach a neuron located at position \mathbf{r} and, in a similar fashion, $J \in C(\bar{\Omega} \times \bar{\Omega})$ represents the strength of this connection. It is natural to assume that the delay τ is non-negative and not identically zero. The function $S \in C^\infty(\mathbb{R})$ is the firing rate function and we assume its k th derivative is bounded for every $k \in \mathbb{N}_0$. $S(V(t, \mathbf{r}))$ hence denotes the firing rate of a neuron at position \mathbf{r} and time t , given the membrane potential $V(t, \mathbf{r})$. Additionally, we assume that $S(0) = 0$, which means that the background activity has been subtracted so that V represents the deviation from the background potential and (NFE) always admits the trivial steady state $V \equiv 0$, which will hereafter be referred to as the background state.

In [21], local bifurcation theory for systems of the type (NFE) is developed. In the present paper, we show how symmetry arguments and residue calculus can be used to simplify the computations of the spectral properties and the evaluation of the normal form coefficients, respectively. This is done hand in hand with an extensive study of two pitchfork–Hopf bifurcations for ‘Wizard hat’ type of connectivity. In [22], the pitchfork–Hopf bifurcation is also treated for a smooth ‘Mexican hat’ connectivity defined by a cosine function. Periodic boundary conditions lead, however, to a completely different spectral problem. In addition, the functional analytic setting is different, but, in principle, that should not matter for dynamics on the center manifold.

In Section 2, we briefly introduce the functional analytic setting needed to cast the delayed neural field equation (NFE) as an abstract delay equation, and finally as an abstract integral equation. In Section 3, we illustrate how the spectrum and resolvent can be computed explicitly for a specific 1D model, with yet very general form of the connectivity J covering the ‘Wizard hat’ case, as well as with the delay $\tau(\mathbf{r}, \mathbf{r}') = \tau_0 + |\mathbf{r} - \mathbf{r}'|$. We show that the spectrum can be decomposed into an ‘even’ and an ‘odd’ part, corresponding to even and odd eigenfunctions respectively. We conclude Section 3 with the locations of two pitchfork–Hopf bifurcation points. We start Section 4 with the critical normal form on the center manifold of a pitchfork–Hopf bifurcation. Subsequently, we illustrate how the normal form coefficients can be evaluated numerically and conclude with the computation and classification of the normal form in our particular examples. In Section 5 we confirm our results by direct simulations using a discretization of (NFE). We conclude with a discussion in Section 6.

2. Functional analytic setting: DDE and AIE reformulations

In this section, we briefly explain how (NFE) can be written as an equivalent Delay Differential Equation and, subsequently, as an Abstract Integral Equation. A more detailed description is given in [21]. Let $Y := C(\bar{\Omega})$ denote the Banach space of real-valued continuous functions on $\bar{\Omega}$ equipped with the supremum norm

$$\|y\|_Y := \sup_{\mathbf{r} \in \bar{\Omega}} |y(\mathbf{r})| \quad (1)$$

$V(t) \in Y$ denotes the spatial distribution of the membrane potential at time t , and we sometimes abuse notation and write $V(t, \mathbf{r})$ to denote $V(t)(\mathbf{r})$. By defining h as the maximal delay

$$h := \sup_{\mathbf{r}, \mathbf{r}' \in \bar{\Omega}} \tau(\mathbf{r}, \mathbf{r}') < \infty \quad (2)$$

the state space $X := C([-h, 0]; Y)$ is the Banach space consisting of continuous Y -valued functions equipped with the supremum norm

$$\|\phi\|_X := \sup_{t \in [-h, 0]} \|\phi(t)\|_Y. \quad (3)$$

By $V_t \in X$ we denote the history of the system at time $t \geq 0$ defined by

$$V_t(\theta) := V(t + \theta) \quad \forall t \geq 0, \theta \in [-h, 0] \quad (4)$$

We also define the nonlinear operator $G : X \rightarrow Y$ by

$$G(\phi)(\mathbf{r}) := \int_{\Omega} J(\mathbf{r}, \mathbf{r}') S(\phi(-\tau(\mathbf{r}, \mathbf{r}'), \mathbf{r}')) d\mathbf{r}'$$

$$\forall \phi \in X, \forall \mathbf{r} \in \bar{\Omega}. \quad (5)$$

Since $\hat{\phi} := 0$ corresponds to the stationary background state $V \equiv 0$, we have

$$G(0) = 0. \quad (6)$$

Proposition 1 ([21, Proposition 11]). *The operator $G : X \rightarrow Y$ is well-defined by (5) and in $C^\infty(X, Y)$. For $k \in \mathbb{N}$ its k th Fréchet derivative $D^k G(\phi) \in \mathcal{L}_k(X, Y)$ in the point $\phi \in X$ is given by*

$$(D^k G(\phi)(\varphi_1, \dots, \varphi_k))(\mathbf{r}) = \int_{\Omega} J(\mathbf{r}, \mathbf{r}') S^{(k)}(\phi(-\tau(\mathbf{r}, \mathbf{r}'), \mathbf{r}')) \prod_{i=1}^k \varphi_i(-\tau(\mathbf{r}, \mathbf{r}'), \mathbf{r}') d\mathbf{r}' \quad (7)$$

for $\varphi_1, \dots, \varphi_k \in X$ and $\mathbf{r} \in \bar{\Omega}$. \square

Now, studying the neural field equation (NFE) is equivalent to analyzing the following Delay Differential Equation:

$$\begin{cases} \dot{V}(t) = F(V_t) & \text{for } t \geq 0 \\ V(t) = \phi(t) & \text{for } t \in [-h, 0] \end{cases} \quad (\text{DDE})$$

where $V : [-h, \infty) \rightarrow Y$ and $\phi \in X$ is the initial condition, while $F : X \rightarrow Y$ is given by

$$F(\phi) := -\alpha \phi(0) + G(\phi) \quad \forall \phi \in X. \quad (8)$$

Definition. A function $x \in C([-h, \infty); Y) \cap C^1([0, \infty); Y)$ that satisfies (DDE) is called its *global solution*.

Lemma 2 ([21, Lemma 3]). *The operator F defined in (8) is globally Lipschitz continuous and k times Fréchet differentiable for any $k = 1, 2, \dots$ \square*

If $F \equiv 0$, then the solution semigroup corresponding to (DDE) is the shift semigroup T_0 , given by

$$(T_0(t)\phi)(\theta) := \begin{cases} \phi(t + \theta) & -h \leq t + \theta \leq 0 \\ \phi(0) & 0 \leq t + \theta \end{cases} \quad (9)$$

for all $\phi \in X$, $t \geq 0$, $\theta \in [-h, 0]$. Let $X^\odot \subset X^*$ be the maximal subspace of strong continuity of the adjoint semigroup T_0^* on the dual space X^* . This space is known as the *sun-dual* of X with respect to T_0 . By the general theory of adjoint semigroups, see e.g. [23, Appendix II.3], it holds that X^\odot is T_0^* -invariant and

$$X^\odot = \overline{D(A_0^*)}, \quad (10)$$

where A_0 is the infinitesimal generator of T_0 and A_0^* is its adjoint. Moreover [24],

$$X^\odot = Y^* \times L^1([0, h]; Y^*), \quad (11)$$

where the second factor is the space of Bochner integrable Y^* -valued functions on $[0, h]$.

Let T_0^\odot be the strongly continuous semigroup on X^\odot obtained by restriction of T_0^* to X^\odot . Again by the general theory of adjoint semigroups, its infinitesimal generator A_0^\odot is

$$D(A_0^\odot) = \{\phi^\odot \in D(A_0^*) : A_0^* \phi^\odot \in X^\odot\}, \quad A_0^\odot \phi^\odot = A_0^* \phi^\odot. \quad (12)$$

Performing this construction once more, this time starting from the strongly continuous semigroup T_0^\odot on the Banach space X^\odot , we obtain the adjoint semigroup $T_0^{\odot*}$ on the dual space $X^{\odot*} = Y^{**} \times [L^1([0, h]; Y^*)]^*$.

The original space X is canonically embedded into $X^{\odot*}$ via $j : X \rightarrow X^{\odot*}$ given by

$$\langle \phi^\odot, j\phi \rangle = \langle \phi, \phi^\odot \rangle \quad \forall \phi \in X, \quad \forall \phi^\odot \in X^\odot, \quad (13)$$

where

$$\langle \phi, \phi^\odot \rangle := \phi^\odot(\phi). \quad (14)$$

Define $E : X \rightarrow X^{\odot*}$ by

$$E(\phi) := (F(\phi), 0) \quad (15)$$

for all $\phi \in X$. E maps into $Y \times \{0\}$ which is a closed subspace of $X^{\odot*}$. Now consider the *Abstract Integral Equation*

$$u(t) = T_0(t)\phi + j^{-1} \int_0^t T_0^{\odot*}(t-s)E(u(s)) ds \quad \forall t \geq 0 \quad (\text{AIE})$$

where $\phi \in X$ is an initial condition, $u \in C([0, \infty); X)$ is the unknown and the convolution integral is of weak* Riemann type, see [23, Section III.1 and Appendix II.3]. Using the representation (11) for X^\odot together with (9) a direct computation shows that, for fixed $t \geq 0$ and $u \in C([0, \infty); X)$,

$$\int_0^t T_0^{\odot*}(t-s)E(u(s)) ds = j\psi \quad (16)$$

where $\psi \in X$ is given by

$$\psi(\theta) := \int_0^{\max(t+\theta, 0)} F(u(s)) ds \quad \forall \theta \in [-h, 0]$$

the integral being of the vector-valued Riemann type. As a consequence, the application of j^{-1} in (AIE) is warranted, since (16) shows that the occurring weak*-integral takes values in the range of j .

The following theorem provides the connection between (DDE) and (AIE). Since F (and consequently E) is globally Lipschitz continuous by Lemma 2, a standard contraction argument shows that (AIE) admits unique global solutions for every initial datum $\phi \in X$. We conclude that (DDE) therefore admits unique global solutions as well.

Theorem 3 ([21, Theorem 6]). *Equivalence of (DDE) and (AIE). The following two statements hold.*

- Suppose that $u \in C([0, \infty); X)$ satisfies (AIE). Define $x : [-h, \infty) \rightarrow Y$ by $x_0 := \phi$ and $x(t) := u(t)(0)$ for $t \geq 0$. Then x is a global solution of (DDE).
- Conversely, suppose that x is a global solution of (DDE). Define $u : [0, \infty) \rightarrow X$ by $u(t) := x_t$. Then $u \in C([0, \infty); X)$ and u satisfies (AIE). \square

To study small deviations from the background state $\hat{\phi} = 0$, it is useful to write

$$F(\phi) = -\alpha\phi(0) + L\phi + \hat{G}(\phi) \quad \forall \phi \in X \quad (17)$$

where $L := DG(0) \in \mathcal{L}(X, Y)$ is the Fréchet derivative of G at $\hat{\phi} = 0$ and $\hat{G} : X \rightarrow Y$ is given by

$$\hat{G}(\phi) := G(\phi) - L\phi \quad \forall \phi \in X.$$

It follows that $\hat{G}(0) = 0$ by (6) as well as $D\hat{G}(0) = 0$, and in this sense \hat{G} contains only non-linear information. Similar to (15), we define the corresponding $X^{\odot*}$ -valued non-linearity $R : X \rightarrow X^{\odot*}$ by

$$R(\phi) := (\hat{G}(\phi), 0) = (G(\phi) - L\phi, 0) \quad (18)$$

for all $\phi \in X$. Clearly R inherits the smoothness of G given by Proposition 1. We also observe that R , like E , maps into the closed subspace $Y \times \{0\}$ of $X^{\odot*}$.

The solution of the *linearized problem*

$$\begin{cases} \dot{V}(t) = -\alpha V(t) + LV_t & \text{for } t \geq 0 \\ V(t) = \phi(t) & \text{for } t \in [-h, 0] \end{cases} \quad (19)$$

defines a strongly continuous semigroup T on X [21, Theorem 8] generated by $A : D(A) \subset X \rightarrow X$ where

$$\begin{aligned} D(A) &= \{\phi \in X : \phi' \in X \text{ and } \phi'(0) = -\alpha\phi(0) + L\phi\}, \\ A\phi &= \phi'. \end{aligned} \quad (20)$$

An argument analogous to that leading to [23, Corollary III.2.8] shows that

$$D(A^*) = D(A_0^*) \quad (21)$$

so by (10), the sun-duals of X with respect to T_0 and T are identical and may both be denoted by X^\odot . Moreover,

$$D(A^\odot) = \{\phi^\odot \in D(A^*) : A^*\phi^\odot \in X^\odot\}, \quad A^\odot = A^*. \quad (22)$$

It also follows that if $\phi \in C^1([-h, 0]; Y)$, then $j\phi \in D(A^{\odot*})$ and

$$A^{\odot*}j\phi = (0, \phi') + (DF(0)\phi, 0) \quad (23)$$

where $DF(0)\phi = -\alpha\phi(0) + L\phi$.

3. Spectral properties of the linearized problem

From now on, we denote by $\rho(A) \subset \mathbb{C}$, $\sigma(A)$ and $\sigma_p(A)$ the resolvent set, the spectrum and the point spectrum of A , respectively. When $z \in \rho(A)$ we write $R(z, A) = (z - A)^{-1}$ for the resolvent of A at z . With L as in (17) and $z \in \mathbb{C}$ we define $L_z \in \mathcal{L}(Y)$ as

$$L_z f := L(\theta \mapsto e^{\theta z} f) \quad (24)$$

for all $f \in Y$ and $\theta \in [-h, 0]$, as well as the characteristic operator $\Delta(z) \in \mathcal{L}(Y)$ by

$$\Delta(z) := z + \alpha - L_z. \quad (25)$$

Proposition 4 ([25, Proposition VI.6.7]). *The complex number $\lambda \in \sigma(A)$ if and only if $0 \in \sigma(\Delta(\lambda))$ and $\psi \in D(A)$ is an eigenvector corresponding to λ if and only if $\psi = \{\theta \mapsto e^{\theta \lambda} q_\lambda\}$ where non-trivial $q_\lambda \in Y$ satisfies $\Delta(\lambda)q_\lambda = 0$. \square*

It can be shown that away from the point $(-\alpha)$, the spectrum consists of isolated eigenvalues of finite type [21, Definition 17 and Corollary 18].

We will now focus on the case of a one-dimensional spatial domain and, following [22], assume that the delays arising in (NFE) consist of two parts. The finite propagation speed of action potentials leads to a conductance delay and due to synaptic processes and dendritic integration there is an additional fixed, 'intrinsic' delay τ_0 . Rescaling space and time such that $\overline{\Sigma} = [-1, 1]$ and the propagation speed is set to 1 then leads to

$$\frac{\partial V}{\partial t}(t, x) = -\alpha V(t, x) + \int_{-1}^1 J(x, y) S(V(t - \tau(x, y), y)) dy \quad (26)$$

where

$$\tau(x, y) = \tau_0 + |x - y| \quad \forall x, y \in [-1, 1]. \quad (27)$$

We choose the connectivity function J to be homogeneous and isotropic and given by a sum of N exponentials

$$J(x, y) = \hat{J}(x - y) = \sum_{j=1}^N \hat{c}_j e^{-\mu_j |x - y|} \quad \forall x, y \in (-1, 1), \quad (28)$$

where $\hat{c}_j, \mu_j \in \mathbb{C}$ are such that J is real.

The firing rate function S is chosen as in [26] to be an odd sigmoid with steepness parameter $r > 0$:

$$S(V) = \frac{1}{1 + e^{-rV}} - \frac{1}{2} \quad \forall V \in \mathbb{R}. \quad (29)$$

Under the above assumptions, a characteristic equation can be formulated and corresponding eigenfunctions and the solution to the resolvent problem can be determined explicitly.

3.1. \mathbb{Z}_2 symmetries

For a general treatment on local bifurcations with symmetry we refer the reader to [27]. For our particular choice of firing rate function (29), system (26) possesses two \mathbb{Z}_2 symmetries generated by involutions $\kappa_{1,2} \in \mathcal{L}(Y)$ defined by

$$\begin{aligned} (\kappa_1 f)(x) &:= f(-x) \\ (\kappa_2 f)(x) &:= -f(-x). \end{aligned} \quad (30)$$

Note that (26) is always equivariant w.r.t. κ_1 , while the symmetry κ_2 appears due to our choice of an odd firing rate S . The fixed subspaces of the involutions κ_1 and κ_2 are composed of even and odd functions, respectively.

If $\tilde{\kappa}_{1,2} \in \mathcal{L}(X)$ are involutions defined by

$$\begin{aligned} (\tilde{\kappa}_1 \phi)(\theta, x) &:= \phi(\theta)(-x) \\ (\tilde{\kappa}_2 \phi)(\theta, x) &:= -\phi(\theta)(-x), \end{aligned} \quad (31)$$

then the (DDE) corresponding to this specific problem has the symmetries

$$\kappa_i F(\phi) = F(\tilde{\kappa}_i \phi) \quad \text{for } i = 1, 2 \quad (32)$$

and the fixed subspaces of $\tilde{\kappa}_i$ in X are invariant sets for (DDE).

3.2. Eigenvalues and eigenfunctions

The Fréchet derivative of G at the background state is given by Proposition 1, namely

$$(DG(0)\phi)(x) = \int_{-1}^1 \hat{f}_0(x-y)\phi(-\tau(x,y), y) dy \quad (33)$$

with

$$\hat{f}_0(x) = \sum_{j=1}^N c_j e^{-\mu_j |x|}, \quad c_j = S'(0)\hat{c}_j. \quad (34)$$

For $z \in \mathbb{C}$, define

$$k_i := z + \mu_i \quad \forall i = 1, \dots, N \quad (35)$$

and the set

$$\mathcal{S} := \{z \in \mathbb{C} : \exists i, j \in \{1, \dots, N\}, i \neq j \text{ such that } k_i^2 = k_j^2\}. \quad (36)$$

Theorem 5 ([21, Theorem 25]). Whenever $z \notin \mathcal{S}$, $\Delta(z)q_z = 0$ implies

$$\beta_0 q_z + \beta_1 q_z^{(2)} + \dots + \beta_{N-1} q_z^{(2N-2)} + \beta_N q_z^{(2N)} = 0 \quad (37)$$

for some unique vector $\beta \in \mathbb{C}^{N+1}$ depending on z and $q_z^{(k)}$ denoting the k th derivative of q_z w.r.t. the spatial variable. \square

Eigenvalues of the linear ODE (37) are roots of the characteristic polynomial \mathcal{P}_z given by the following proposition.

Proposition 6 ([21, Proposition 26]). For $z \notin \mathcal{S}$ the characteristic polynomial \mathcal{P}_z of (37) is given by

$$\begin{aligned} \mathcal{P}_z(\rho) &= \frac{e^{z\tau_0}(z + \alpha)}{2} \prod_{j=1}^N (\rho^2 - k_j(z)^2) \\ &\quad + \sum_{i=1}^N c_i k_i(z) \prod_{\substack{j=1 \\ j \neq i}}^N (\rho^2 - k_j(z)^2). \quad \square \end{aligned} \quad (38)$$

Analysis of the characteristic polynomial results in the following two statements.

Proposition 7. If the characteristic polynomial \mathcal{P}_z has $2N$ distinct roots for some $z \in \mathbb{C}$, then $k_i(z) \neq 0$ for all $i = 1, \dots, N$.

Proof. Assume that $k_l(z) = 0$ for some $l \in \{1, \dots, N\}$. Without loss of generality one sets $l = N$ and (38) becomes:

$$\begin{aligned} \mathcal{P}_z(\rho) &= \frac{e^{z\tau_0}(z + \alpha)}{2} \rho^2 \prod_{j=1}^{N-1} (\rho^2 - k_j(z)^2) \\ &\quad + \sum_{i=1}^{N-1} c_i k_i(z) \rho^2 \prod_{\substack{j=1 \\ j \neq i}}^{N-1} (\rho^2 - k_j(z)^2). \end{aligned} \quad (39)$$

All terms share a common factor ρ^2 and hence the polynomial has a double root at $\rho = 0$. Since the order of \mathcal{P}_z is $2N$, it can at most have $2N - 2$ other roots away from 0. Therefore, the initial assumption is incorrect and $k_i(z) \neq 0$ for all i . \square

Proposition 8. If $z \notin \mathcal{S}$ and the characteristic polynomial \mathcal{P}_z has $2N$ distinct roots $\pm \rho_1(z), \dots, \pm \rho_N(z)$, then $k_j(z) \neq \pm \rho_i(z)$ for all $i, j = 1, \dots, N$.

Proof. The result follows naturally if it is shown that $\mathcal{P}_z(k_l) \neq 0$ for all $l = 1, \dots, N$. Without loss of generality, it suffices to only consider $l = N$.

$$\begin{aligned} \mathcal{P}_z(k_N) &= \frac{e^{z\tau_0}(z + \alpha)}{2} \prod_{j=1}^N (k_N^2 - k_j^2) + \sum_{i=1}^N c_i k_i \prod_{\substack{j=1 \\ j \neq i}}^N (k_N^2 - k_j^2) \\ &= c_N k_N \prod_{j=1}^{N-1} (k_N^2 - k_j^2). \end{aligned} \quad (40)$$

Since $z \notin \mathcal{S}$, all terms in the product are non-zero. By definition, $c_N \neq 0$ and from Proposition 7 follows $k_N \neq 0$, hence $\mathcal{P}_z(k_N) \neq 0$. \square

Proposition 9 ([21, Proposition 27]). If $z \notin \mathcal{S}$ and the characteristic polynomial \mathcal{P}_z has $2N$ distinct roots $\pm \rho_1(z), \dots, \pm \rho_N(z)$, then the general solution of (37) is of the form

$$q_z(x) = \sum_{i=1}^N \left[a_i \cosh(\rho_i(z)x) + b_i \sinh(\rho_i(z)x) \right] \quad (41)$$

where the coefficients $a_i, b_i \in \mathbb{C}$ are arbitrary. \square

In this particular case, the characteristic operator $\Delta(z)$ defined in (25) is given by

$$\begin{aligned} (\Delta(z)q)(x) &= (z + \alpha)q(x) - e^{-z\tau_0} \\ &\quad \times \int_{-1}^1 \hat{f}_0(x-y) e^{-z|x-y|} q(y) dy \end{aligned} \quad (42)$$

for all $z \in \mathbb{C}$, $q \in Y$ and $x \in \overline{\Omega} = [-1, 1]$.

So for (41) to satisfy $\Delta(z)q_z = 0$, there must hold

$$\begin{aligned} 0 &= e^{z\tau_0}(z + \alpha) \sum_{i=1}^N \left[a_i \cosh(\rho_i x) + b_i \sinh(\rho_i x) \right] \\ &\quad - \sum_{j=1}^N c_j \sum_{i=1}^N \int_{-1}^1 e^{-k_j|x-y|} \left[a_i \cosh(\rho_i y) + b_i \sinh(\rho_i y) \right] dy \end{aligned} \quad (43)$$

for all $x \in \overline{\Omega}$. For notational convenience we have suppressed the dependence of ρ_i and k_j on z . Splitting the domains of integration and sorting the terms yields

$$\begin{aligned} 0 &= \sum_{i=1}^N \left\{ a_i \cosh(\rho_i x) \left[e^{z\tau_0}(z + \alpha) - \sum_{j=1}^N \frac{2c_j k_j}{k_j^2 - \rho_i^2} \right] \right. \\ &\quad \left. + b_i \sinh(\rho_i x) \left[e^{z\tau_0}(z + \alpha) - \sum_{j=1}^N \frac{2c_j k_j}{k_j^2 - \rho_i^2} \right] \right\} \end{aligned}$$

$$\begin{aligned}
& + \sum_{j=1}^N c_j e^{-k_j} \left\{ e^{k_j x} \left[\sum_{i=1}^N a_i [S_z^e]_{j,i} + \sum_{i=1}^N b_i [S_z^o]_{j,i} \right] \right. \\
& \left. + e^{-k_j x} \left[\sum_{i=1}^N a_i [S_z^e]_{j,i} - \sum_{i=1}^N b_i [S_z^o]_{j,i} \right] \right\} \quad (44)
\end{aligned}$$

where the dependence of k_j and ρ_i on z is again suppressed for simplicity and

$$\begin{aligned}
[S_z^e]_{j,i} &:= \frac{k_j(z) \cosh(\rho_i(z)) + \rho_i(z) \sinh(\rho_i(z))}{k_j(z)^2 - \rho_i(z)^2} \\
[S_z^o]_{j,i} &:= \frac{k_j(z) \sinh(\rho_i(z)) + \rho_i(z) \cosh(\rho_i(z))}{k_j(z)^2 - \rho_i(z)^2}. \quad (45)
\end{aligned}$$

Proposition 6 guarantees that the first two lines in (44) vanish when $z \notin \mathcal{S}$. With $a = [a_1, a_2, \dots, a_N]$ and $b = [b_1, b_2, \dots, b_N]$ the last two lines in (44) vanish if and only if

$$\begin{bmatrix} S_z^e & 0 \\ 0 & S_z^o \end{bmatrix} \begin{bmatrix} a \\ b \end{bmatrix} = 0 \quad (46)$$

where S_z^e and S_z^o are given by (45). System (46) has a non-trivial solution if and only if

$$\det(S_z^e) \det(S_z^o) = 0. \quad (47)$$

These results are summarized in the following theorem.

Theorem 10 ([21, Theorem 28]). Suppose that $\lambda \notin \mathcal{S}$ and the characteristic polynomial \mathcal{P}_λ has $2N$ distinct roots, denoted by $\pm \rho_i(\lambda)$ for $i = 1, \dots, N$, then λ is an eigenvalue of A if and only if

$$\det(S_\lambda^e) \det(S_\lambda^o) = 0. \quad (48)$$

Furthermore, $\{\theta \mapsto e^{\theta \lambda} q_\lambda\} \in X$ is a corresponding eigenfunction, where $q_\lambda \in Y$ has the form (41). The coefficients $a = [a_1, a_2, \dots, a_N]$ and $b = [b_1, b_2, \dots, b_N]$ are a non-trivial solution of the system of equations

$$\begin{bmatrix} S_\lambda^e & 0 \\ 0 & S_\lambda^o \end{bmatrix} \begin{bmatrix} a \\ b \end{bmatrix} = 0. \quad \square \quad (49)$$

Corollary 11. Suppose the same conditions as in Theorem 10 hold and that λ is a simple eigenvalue. Then the eigenfunction corresponding to λ is even w.r.t. the spatial variable if $\det(S_\lambda^e) = 0$ and odd w.r.t. the spatial variable if $\det(S_\lambda^o) = 0$.

Proof. Suppose that $\det(S_\lambda^e) = 0$. From the fact that λ is a simple eigenvalue then follows that $\det(S_\lambda^o) \neq 0$. Therefore, there is no non-trivial solution to $S_\lambda^o b = 0$ and we can conclude that q_λ is even. The odd case is similar. \square

Using the involutions defined by (31), we see that if an eigenfunction ψ corresponding to an eigenvalue λ is even or odd w.r.t. the spatial variable, it satisfies $\tilde{\kappa}_2 \psi = -\psi$ or $\tilde{\kappa}_1 \psi = -\psi$, respectively.

3.3. Example: pitchfork–Hopf bifurcations for ‘Wizard hat’ connectivity

In the following example, we set $\alpha = 1$ and choose the connectivities (see Fig. 1)

$$\hat{J}_1(x) = 12.5e^{-2|x|} - 10e^{-|x|} \quad (50a)$$

$$\hat{J}_2(x) = 12e^{-3|x|} - 10e^{-|x|}. \quad (50b)$$

This type of connectivity models a mixed population of interacting excitatory and inhibitory neurons with local excitation and distal

Table 1

Parameter values corresponding to pitchfork–Hopf bifurcations of the background state.

Parameter	α	\hat{c}_1	\hat{c}_2	μ_1	μ_2	r	τ_0
κ_1 -pitchfork–Hopf	1	12.5	−10	2	1	2.5169	2.5939
κ_2 -pitchfork–Hopf	1	12	−10	3	1	2.5102	0.3178

inhibition. While the inhibitory part is the same for both connectivities, excitation is a bit weaker and decays faster for connectivity \hat{J}_2 . Parameters in the system are r , the steepness of the firing rate function, and the fixed delay τ_0 .

Since $N = 2$, the characteristic polynomial $\mathcal{P}_z(\rho)$ in (38) is a second order polynomial in ρ^2 . We can therefore explicitly determine the characteristic equation

$$\det(S_z^e) \det(S_z^o) = 0. \quad (51)$$

This enables us to numerically find values of z which solve (51). Suppose λ is such a root. If $\lambda \notin \mathcal{S}$ and the numbers $\pm \rho_{1,2}(\lambda)$ are all distinct, we can conclude from Theorem 10 that λ is an eigenvalue, and we can classify this eigenvalue as being either ‘even’ or ‘odd’, depending on whether $\det(S_\lambda^e) = 0$ or $\det(S_\lambda^o) = 0$. Similarly, bifurcation points can be located by solving for parameter values at which there is an eigenvalue on the imaginary axis.

In our specific example, we find zero eigenvalues in the spectrum of the background state at approximately $r = 2.5169$ and $r = 2.8020$ for connectivity (50a) and at approximately $r = 2.5102$ and $r = 2.8146$ for connectivity (50b). These values are independent of the second parameter since τ_0 only influences the delays in (19). By varying τ_0 we can also find a pair of imaginary eigenvalues (a Hopf singularity) for a fixed value of r . Continuation of this bifurcation leads to the bifurcation diagrams shown in Fig. 2. The eigenvalues at the (first) zero-Hopf points are shown in Fig. 3.

The critical eigenvalues

$$\lambda_1^{(1)} = 0, \quad \lambda_1^{(2)} = 0$$

belonging to connectivities (50a) and (50b) are in the ‘odd’ and ‘even’ part of the spectrum respectively, which means that their corresponding (real-valued) eigenfunctions can be written as

$$\psi_1^{(1)}(t, x) = b_1 \sinh(\rho_1^{(1)} x) + b_2 \sinh(\rho_2^{(1)} x) \quad (52a)$$

$$\psi_1^{(2)}(t, x) = a_1 \cosh(\rho_1^{(2)} x) + a_2 \cosh(\rho_2^{(2)} x) \quad (52b)$$

where we have suppressed the dependence of a_i, b_i and ρ on λ . Computations yield

$$\begin{aligned}
\rho_1^{(1)} &= 3.4590i, & \rho_2^{(1)} &= 1.3828i, \\
b_1 &= -0.5281i, & b_2 &= -0.3440i, \\
\rho_1^{(2)} &= 4.2985i, & \rho_2^{(2)} &= 2.0384i, \\
a_1 &= 0.6323, & a_2 &= 0.2605.
\end{aligned} \quad (53)$$

The results are visualized in Fig. 4. In particular, they imply that zero eigenvalue $\lambda_1^{(1)}$ corresponds to a pitchfork bifurcation of the κ_1 -symmetric background solution while zero eigenvalue $\lambda_1^{(2)}$ corresponds to a pitchfork bifurcation of the κ_2 -symmetric background solution [28, Theorem 7.7]. We will therefore refer to them as κ_1 -pitchfork and κ_2 -pitchfork bifurcations respectively.

The imaginary critical eigenvalues

$$\lambda_2^{(1)} = 0.6877i, \quad \lambda_2^{(2)} = 1.9706i \quad (54)$$

are both in the ‘even’ part of the point spectrum, which means that their corresponding eigenfunctions ψ are even functions in space and can be written as

$$\psi_2(t, x) = e^{\lambda_2 t} [a_1 \cosh(\rho_1 x) + a_2 \cosh(\rho_2 x)]. \quad (55)$$

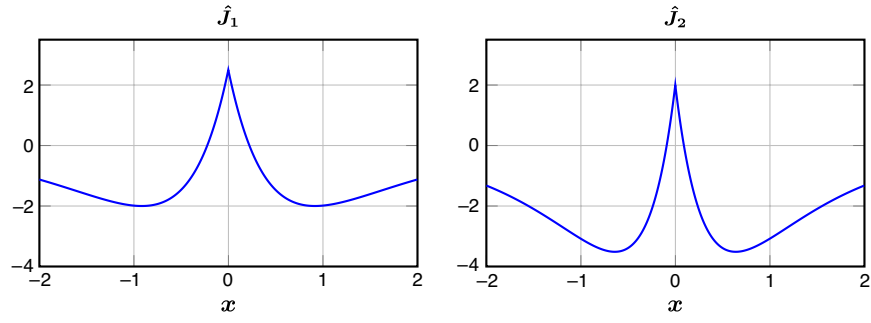


Fig. 1. ‘Wizard hat’ connectivity functions $\hat{J}_1(x)$ and $\hat{J}_2(x)$.

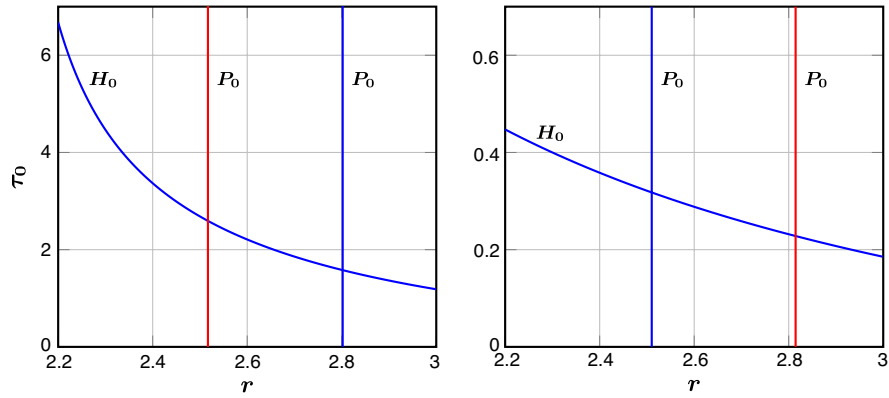


Fig. 2. Bifurcation curves for the background state: H_0 corresponds to a Hopf and P_0 to a pitchfork bifurcation. ‘Even’ bifurcations are shown in *blue*, while ‘odd’ bifurcations are shown in *red*. The background state is stable in the lower-left parameter regions. (For interpretation of the references to color in this figure legend, the reader is referred to the web version of this article.)

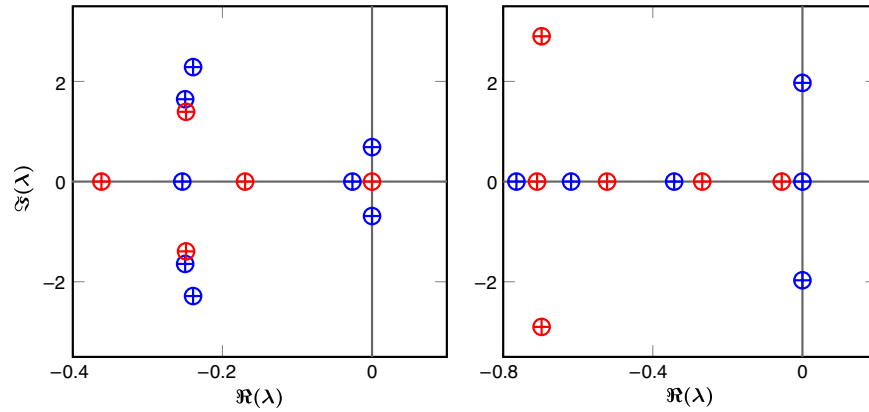


Fig. 3. Spectra at the pitchfork–Hopf bifurcations. ‘Even’ eigenvalues are shown in *blue*, while ‘odd’ eigenvalues are shown in *red*. Corresponding parameter values are given in Table 1. (For interpretation of the references to color in this figure legend, the reader is referred to the web version of this article.)

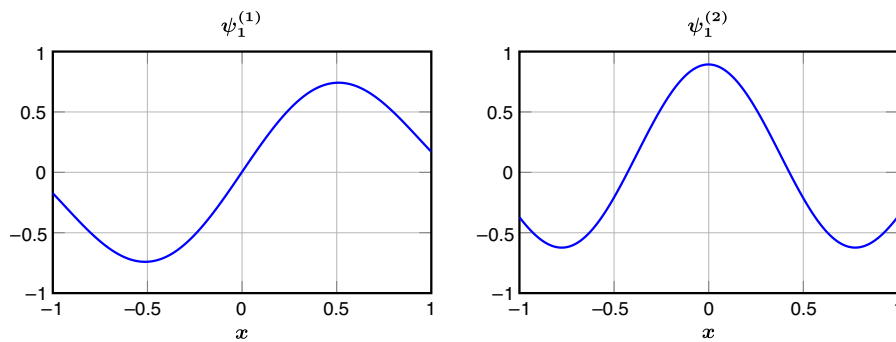


Fig. 4. Real eigenfunctions $\psi_1^{(1)}$ and $\psi_1^{(2)}$ given by (52) and (53).

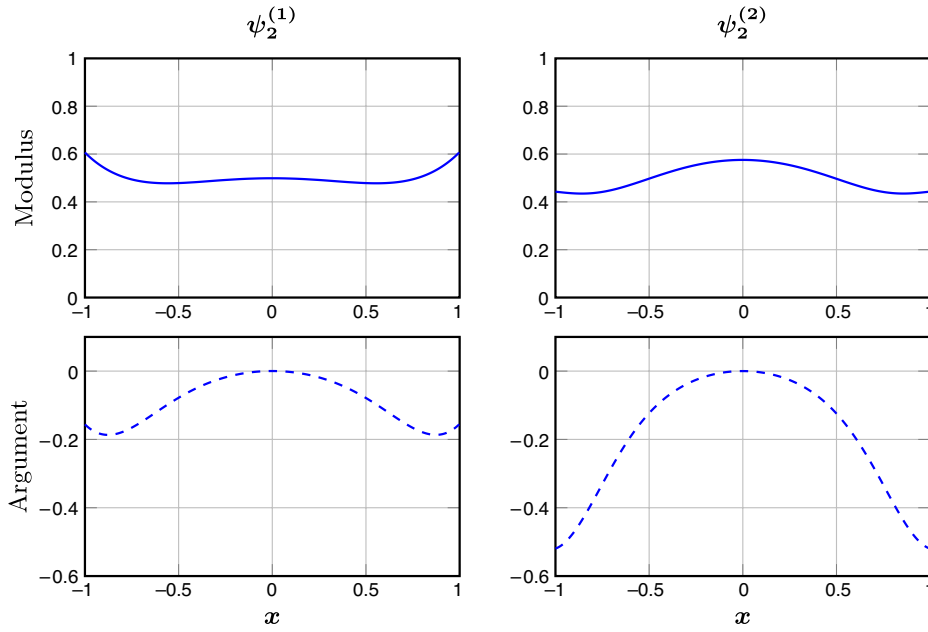


Fig. 5. Complex eigenfunctions $\psi_2^{(1)}$ and $\psi_2^{(2)}$ given by (54)–(56).

Now, computations yield

$$\begin{aligned} \rho_1^{(1)} &= 4.2893 + 1.9087i, & \rho_2^{(1)} &= 0.1813 - 0.7949i, \\ a_1^{(1)} &= 0.0031 + 0.0059i, & a_2^{(1)} &= -0.5014, \\ \rho_1^{(2)} &= 4.1814 + 3.7563i, & \rho_2^{(2)} &= 0.3312 - 1.0759i, \\ a_1^{(2)} &= 0.0016 - 0.0028i, & a_2^{(2)} &= -0.5772. \end{aligned} \quad (56)$$

The results are visualized in Fig. 5. The intersection of the curves P_0 and H_0 gives rise to a *pitchfork–Hopf bifurcation*, provided appropriate normal form coefficients do not vanish.

4. Normal forms on the center manifold

4.1. Critical center manifold

Suppose $\sigma(A)$ contains a simple zero eigenvalue and a simple pair of purely imaginary eigenvalues

$$\lambda_1 = 0, \quad \lambda_{2,3} = \pm i\omega$$

with $\omega > 0$, and no other eigenvalues on the imaginary axis. Let $\psi_{1,2}$ and $\psi_{1,2}^\circ$ be the corresponding eigenfunctions of A and A^* ,

$$A\psi_1 = 0, \quad A\psi_2 = i\omega\psi_2, \quad A^*\psi_1^\circ = 0, \quad A^*\psi_2^\circ = i\omega\psi_2^\circ.$$

It is always possible to scale these vectors such that the ‘bi-orthogonality’ relation

$$\langle \psi_j, \psi_i^\circ \rangle = \delta_{ij} \quad i, j \in \{1, 2\}$$

holds. The center subspace X_0 is spanned by some basis Ψ of eigenvectors corresponding to the critical eigenvalues of A . In our case Ψ is given by

$$\Psi = \{\psi_1, \psi_2, \bar{\psi}_2\} \quad (57)$$

with ψ_1, ψ_2 defined by (52), (55) and shown in Figs. 4 and 5 respectively. If $\xi \in X_0$, then

$$\xi = w\psi_1 + z\psi_2 + \bar{z}\bar{\psi}_2 \quad (58)$$

for some $w \in \mathbb{R}$ and $z \in \mathbb{C}$. Both involutions κ_1 and κ_2 act on X_0 as reflection, i.e.

$$(w, z) \rightarrow (-w, -z). \quad (59)$$

We recall Theorem 3 from Section 2, which established the equivalence of (DDE) and (AIE). The latter equation is a variation-of-constants formula in the state space X , for which a locally invariant critical center manifold $\mathcal{W}_{loc}^c \subset X$ may be constructed using the same standard fixed-point approach taken in [23, Chapter IX]. This, then, is one of the advantages of reformulating (DDE) as an abstract integral equation.

We would like to point out that a center manifold result for neural field equations in a Hilbert space setting was presented in [29]. Unfortunately, there are issues with some of the proofs [29, Lemma C.1] that we have communicated to the authors, also see [21, Section 2.4]. These have been confirmed and we have understood that an erratum will be submitted for publication.

We now return to our discussion of the critical center manifold, for which one has the formal expansion

$$\mathcal{H}(w, z, \bar{z}) = w\psi_1 + z\psi_2 + \bar{z}\bar{\psi}_2 + \sum_{j+k+l \geq 2} \frac{1}{j!k!l!} h_{jkl} w^j z^k \bar{z}^l. \quad (60)$$

By weak* differentiation of (AIE), and exploiting the finite dimensionality of \mathcal{W}_{loc}^c , one shows that the solution of (AIE) satisfies the abstract ODE

$$\dot{u}(t) = j^{-1}(A^\circ * ju(t) + R(u(t))) \quad \forall t \in \mathbb{R} \quad (61)$$

where the non-linearity $R : X \rightarrow X^{\circ*}$ is given by (18).

Let $\xi(t)$ be the projection of $u(t)$ onto the center subspace X_0 . Then the coordinates of $\xi(t)$ satisfy an ODE that is equivariant w.r.t. the transformation (59), cf. [28, Theorem 7.6]. It is well known that such ODE is smoothly equivalent to the *Poincaré normal form*

$$\begin{cases} \dot{w} = g_{300}w^3 + g_{111}w|z|^2 + \mathcal{O}(|w, z, \bar{z}|^5) \\ \dot{z} = i\omega z + g_{210}zw^2 + g_{021}z|z|^2 + \mathcal{O}(|w, z, \bar{z}|^5) \end{cases} \quad (62)$$

where $w \in \mathbb{R}$, $z \in \mathbb{C}$ [30]. In (62), the coefficients g_{300} and g_{111} are real-valued, while g_{210} and g_{021} are complex-valued.

4.2. The canonical pitchfork–Hopf bifurcation

As we have just seen, the restriction of (NFE) to the critical center manifold is equivalent to the symmetric normal form (62). By

Table 2

[30, Table 7.5.2] Different unfoldings of (65).

Case	Ia	Ib	II	III	IVa	IVb	V	VIa	VIb	VIIa	VIIb	VIII
d	+1	+1	+1	+1	+1	+1	−1	−1	−1	−1	−1	−1
b	+	+	+	−	−	−	+	+	+	−	−	−
c	+	+	−	+	−	−	+	−	−	+	+	−
$1 - bc$	+	−	(+)	(−)	+	−	(−)	+	−	+	−	(−)

Table 3

Classification of fixed points and solution correspondence.

Amplitude solution	Mean field solution
Trivial fixed point (0, 0)	Background state
Mode one fixed point (\bar{w} , 0)	Stationary solution
Mode two fixed point (0, \bar{r})	Oscillation around the background state
Mixed mode fixed point (\bar{w} , \bar{r})	Oscillation around a non-trivial state

substituting $z = re^{i\theta}$ we can conveniently write (62) in cylindrical polar coordinates as

$$\begin{cases} \dot{w} = p_{11}w^3 + p_{12}wr^2 + \mathcal{O}(|w, r|^5) \\ \dot{r} = p_{21}rw^2 + p_{22}r^3 + \mathcal{O}(|w, r|^5) \\ \dot{\theta} = \omega + \mathcal{O}(|w, r|^2) \end{cases} \quad (63)$$

where

$$p_{11} = g_{300}, \quad p_{12} = g_{111}, \quad p_{21} = \text{Re}(g_{210}), \\ p_{22} = \text{Re}(g_{021})$$

and the higher order terms depend smoothly and periodically on θ . We assume that $p_{ij} \neq 0$ for $i, j \in \{1, 2\}$ and $p_{11}p_{22} - p_{12}p_{21} \neq 0$.

If we drop the higher order terms in (63), the first two equations become independent of the third one, which describes rotations around the w -axis. Thus, we can decouple the azimuthal component of (63). Perturbing the first two equations with $\epsilon_1 w$ and $\epsilon_2 r$ respectively leads to the *amplitude equations*

$$\begin{cases} \dot{w} = w(\epsilon_1 + p_{11}w^2 + p_{12}r^2) \\ \dot{r} = r(\epsilon_2 + p_{21}w^2 + p_{22}r^2). \end{cases} \quad (64)$$

The amplitude equations (64) are identical to the amplitude equations of the double Hopf bifurcation studied in [30,28].

The number of parameters in (64) can be reduced by rescaling the variables. By allowing a reversal of time we can assume, without loss of generality, that $p_{11} < 0$. Setting $\hat{w} = \sqrt{-p_{11}}w$, $\hat{r} = \sqrt{|p_{22}|}r$ and dropping the hats lead to

$$\begin{cases} \dot{w} = w(\epsilon_1 - w^2 - br^2) \\ \dot{r} = r(\epsilon_2 - cw^2 - dr^2) \end{cases} \quad (65)$$

where

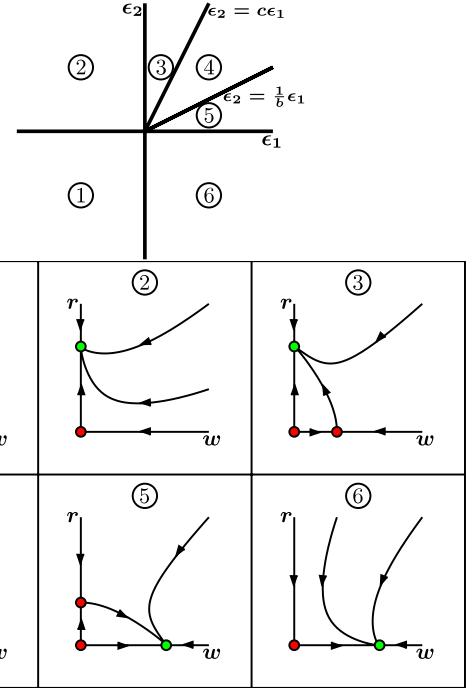
$$b = -\frac{p_{12}}{|p_{22}|}, \quad c = \frac{p_{21}}{p_{11}}, \quad d = \pm 1. \quad (66)$$

Since the system is symmetric in both w and r , we can restrict to $w, r \geq 0$.

Following [30], the unfolding (65) can be classified into twelve topologically different cases, see Table 2.

In [28], the first six unfoldings listed in Table 2 are called the ‘simple’ case, since (65) cannot have limit cycles for $p_{11}p_{22} > 0$. In these cases, the truncation can be justified; the appearing bifurcation diagrams are not affected by the higher order terms.

Depending on the values of b, c and the region in parameter space (ϵ_1, ϵ_2) , the amplitude equations (65) can have up to four different fixed points, which are classified in Table 3. In our two particular examples the non-trivial stationary solutions are of different parity: for κ_1 -pitchfork–Hopf bifurcations the mode one fixed point is odd, while it is even in the case of κ_2 -pitchfork–Hopf bifurcations.

**Fig. 6.** Bifurcation diagram for case Ib.

We conclude this subsection with the parametric portrait and corresponding phase portraits of unfolding Ib, shown in Fig. 6. The characteristic feature of this unfolding is the existence of a bistable region, in which a mode one and a mode two fixed point coexist.

4.3. Normal form coefficients and their practical computation

The critical center manifold \mathcal{W}_{loc}^C has the expansion (60) and by the time-invariance of \mathcal{W}_{loc}^C we have

$$\mathcal{H}(w(t), z(t), \bar{z}(t)) = u(t) \quad \forall t \in \mathbb{R}. \quad (67)$$

Differentiating both sides of (67) with respect to time and using (61), leads to the *homological equation*

$$A^{\odot*}j\mathcal{H}(w, z, \bar{z}) + R(\mathcal{H}(w, z, \bar{z})) = j(\mathcal{H}_w(w, z, \bar{z})\dot{w} + \mathcal{H}_z(w, z, \bar{z})\dot{z} + \mathcal{H}_{\bar{z}}(w, z, \bar{z})\dot{\bar{z}}). \quad (68)$$

Due to our particular choice of an odd firing rate function, the second derivative of the nonlinearity $R: X \rightarrow X^{\odot*}$ vanishes and it may therefore be expanded as

$$R(\phi) = \frac{1}{6}C(\phi, \phi, \phi) + \mathcal{O}(\|\phi\|^4) \quad (69)$$

where $C \in \mathcal{L}_3(X, X^{\odot*})$ is defined by

$$C(\phi_1, \phi_2, \phi_3) := D^3R(0)(\phi_1, \phi_2, \phi_3). \quad (70)$$

We can derive expressions for the critical normal form coefficients as in [21], namely, by substituting the expansions (60), (69), and normal form (62) into the homological equation (68) and equating coefficients of the corresponding powers of u, z, \bar{z} . This leads to linear operator equations of the form

$$(\lambda - A^{\odot*}) \phi^{\odot*} = \psi^{\odot*} \quad (71)$$

where $\lambda \in \mathbb{C}$ and $\psi^{\odot*} \in X^{\odot*}$ is given. Using Fredholm solvability conditions [21, Lemma 33], this results in

$$\begin{aligned} g_{300} &= \frac{1}{6} \langle \psi_1^{\odot}, C(\psi_1, \psi_1, \psi_1) \rangle = \frac{1}{6} \langle \psi_1^{\odot}, (y_{11}, 0) \rangle \\ g_{111} &= \langle \psi_1^{\odot}, C(\psi_1, \psi_2, \bar{\psi}_2) \rangle = \langle \psi_1^{\odot}, (y_{12}, 0) \rangle \\ g_{210} &= \frac{1}{2} \langle \psi_2^{\odot}, C(\psi_2, \psi_1, \psi_1) \rangle = \frac{1}{2} \langle \psi_2^{\odot}, (y_{21}, 0) \rangle \\ g_{021} &= \frac{1}{2} \langle \psi_2^{\odot}, C(\psi_2, \psi_2, \bar{\psi}_2) \rangle = \frac{1}{2} \langle \psi_2^{\odot}, (y_{22}, 0) \rangle \end{aligned} \quad (72)$$

where

$$\begin{aligned} y_{11} &:= D^3 G(0)(\psi_1, \psi_1, \psi_1) \\ y_{12} &:= D^3 G(0)(\psi_1, \psi_2, \bar{\psi}_2) \\ y_{21} &:= D^3 G(0)(\psi_2, \psi_1, \psi_1) \\ y_{22} &:= D^3 G(0)(\psi_2, \psi_2, \bar{\psi}_2) \end{aligned} \quad (73)$$

with $D^3 G(0)$ given by Proposition 1

$$\begin{aligned} (D^3 G(0)(\phi_1, \phi_2, \phi_3))(x) \\ = -\frac{r^3}{8} \int_{-1}^1 \hat{J}(x-y) \prod_{i=1}^3 \phi_i(-\tau(x, y), y) dy. \end{aligned} \quad (74)$$

The normal form coefficients (72) involve pairings of the form $\langle \psi^{\odot}, \phi^{\odot*} \rangle$, for $\psi^{\odot} \in X^{\odot}$, $\phi^{\odot*} \in X^{\odot*}$. It is generally not clear how elements in the spaces

$$X^{\odot} = Y^* \times L^1([0, h]; Y^*)$$

$$X^{\odot*} = Y^{**} \times L^1([0, h]; Y^*)^*$$

are to be expressed numerically and, consequently, how to evaluate pairings involving these elements.

Now suppose that $\lambda \in \sigma_p(A)$ is a simple eigenvalue with corresponding eigenfunction $\psi \in D(A)$. Furthermore, let $\psi^{\odot} \in D(A^*)$ be the eigenfunction of A^* corresponding to λ such that, without loss of generality, $\langle \psi, \psi^{\odot} \rangle = 1$. Let P^{\odot} and $P^{\odot*}$ be the spectral projections on X^{\odot} and $X^{\odot*}$ respectively. It is obvious that $P^{\odot*} \phi^{\odot*} = \nu j \psi$ for some $\nu \in \mathbb{C}$. Though ψ^{\odot} is unknown, the following holds:

$$\begin{aligned} \langle \psi^{\odot}, \phi^{\odot*} \rangle &= \langle P^{\odot} \psi^{\odot}, \phi^{\odot*} \rangle \\ &= \langle \psi^{\odot}, P^{\odot*} \phi^{\odot*} \rangle = \nu \langle \psi^{\odot}, j \psi \rangle = \nu. \end{aligned} \quad (75)$$

Hence we seek to determine ν .

From the Dunford integral representation follows that

$$P^{\odot*} \phi^{\odot*} = \frac{1}{2\pi i} \oint_{\partial C_\lambda} R(z, A^{\odot*}) \phi^{\odot*} dz = \nu j \psi \quad (76)$$

where C_λ is a sufficiently small open disk centered at λ and ∂C_λ its boundary.

All second arguments in the pairings (72) of the normal form coefficients are in $Y \times \{0\} \subseteq X^{\odot*}$, so further analysis can be restricted to elements in this space only. Indeed, since $E : X \rightarrow X^{\odot*}$ as defined in (15) maps into $Y \times \{0\}$, $\phi^{\odot*}$ is of the form $(y, 0)$ for some $y \in Y$. We can therefore find ν by applying Lemma 36 in [21], which we now restate for completeness.

Lemma 12 ([21, Lemma 36]). Suppose that $z \in \rho(A)$. For each $y \in Y$ the function $\varphi = \{\theta \mapsto e^{\theta z} \Delta(z)^{-1} y\}$ is the unique solution in $C^1([-h, 0]; Y)$ of the system

$$\begin{cases} z\varphi(0) - DF(0)\varphi = y \\ z\varphi - \varphi' = 0. \end{cases} \quad (77)$$

Moreover, $\varphi^{\odot*} = j\varphi$ is the unique solution in $D(A^{\odot*})$ of $(z - A^{\odot*}) \varphi^{\odot*} = (y, 0)$, i.e. $\varphi^{\odot*} = R(z, A^{\odot*})(y, 0)$. \square

Lemma 12 enables us to reduce (76) to the Y -valued identity

$$\frac{1}{2\pi i} \oint_{\partial C_\lambda} \Delta(z)^{-1} y dz = \nu \psi(0). \quad (78)$$

We see that we first need to solve an integral equation for $q_z := \Delta(z)^{-1} y \in Y$, in our particular case

$$\begin{aligned} (z + \alpha) q_z(x) - \int_{-1}^1 \hat{J}_0(x-r) e^{-z\tau_0 - z|x-r|} q_z(r) dr &= y(x) \\ \forall x \in \bar{\Omega}. \end{aligned} \quad (79)$$

Inspired by (41) we propose the following variation-of-constants Ansatz for its solution

$$\begin{aligned} q_z(x) &= \frac{y(x)}{\alpha + z} \\ &+ \sum_{i=1}^N \left[a_i(x) \cosh(\rho_i(z)x) + b_i(x) \sinh(\rho_i(z)x) \right]. \end{aligned} \quad (80)$$

Since eigenfunctions $\psi \in X$ are either even or odd w.r.t. the spatial variable, the same holds for $y \in Y$ and this prescribes the parity of the unknown coefficients $a_i, b_i \in Y$. In particular, for even $y \in Y$ there holds that $a_i \in Y$ is even and $b_i \in Y$ is odd for all $i = 1, \dots, N$, and for odd $y \in Y$ it is the other way around.

Substituting Ansatz (80) into (79) and integrating by parts leads to

$$\begin{aligned} 0 &= \sum_{i=1}^N a_i(x) \cosh(\rho_i x) \left[e^{z\tau_0} (z + \alpha) - \sum_{j=1}^N \frac{2c_j k_j}{k_j^2 - \rho_i^2} \right] \\ &+ \sum_{i=1}^N b_i(x) \sinh(\rho_i x) \left[e^{z\tau_0} (z + \alpha) - \sum_{j=1}^N \frac{2c_j k_j}{k_j^2 - \rho_i^2} \right] \\ &+ \sum_{j=1}^N c_j e^{-k_j} \int_{-1}^x e^{k_j r} \left[\frac{-y(r)}{z + \alpha} + \sum_{i=1}^N \frac{a'_i(r)}{k_j^2 - \rho_i^2} \right. \\ &\times (k_j \cosh(\rho_i r) - \rho_i \sinh(\rho_i r)) \\ &+ \sum_{i=1}^N \frac{b'_i(r)}{k_j^2 - \rho_i^2} (k_j \sinh(\rho_i r) - \rho_i \cosh(\rho_i r)) \Big] dr \\ &- \sum_{j=1}^N c_j e^{k_j} \int_x^1 e^{-k_j r} \left[\frac{y(r)}{z + \alpha} + \sum_{i=1}^N \frac{a'_i(r)}{k_j^2 + \rho_i^2} \right. \\ &\times (k_j \cosh(\rho_i r) + \rho_i \sinh(\rho_i r)) \\ &+ \sum_{i=1}^N \frac{b'_i(r)}{k_j^2 - \rho_i^2} (k_j \sinh(\rho_i r) + \rho_i \cosh(\rho_i r)) \Big] dr \\ &+ \sum_{j=1}^N c_j e^{-k_j(1+x)} \left[\sum_{i=1}^N a_i(-1) [S_z^e]_{j,i} - \sum_{i=1}^N b_i(-1) [S_z^o]_{j,i} \right] \\ &+ \sum_{j=1}^N c_j e^{-k_j(1-x)} \left[\sum_{i=1}^N a_i(1) [S_z^e]_{j,i} + \sum_{i=1}^N b_i(1) [S_z^o]_{j,i} \right] \end{aligned} \quad (81)$$

where we have suppressed the dependence of k_j and ρ_i on z and S_z^e, S_z^o are given by (45).

When $z \notin \mathcal{S}$, Proposition 6 guarantees that the first two lines in (81) vanish. We seek functions a_i, b_i such that the integrands and the remaining terms in (81) also vanish. The last two lines in (81) give rise to a boundary condition for the unknown coefficients $a_i, b_i \in Y$. Using their known parity, we see that the last two lines in (81) vanish if and only if

$$S_z^e a(1) + S_z^o b(1) = 0 \quad (82)$$

where $a(x) = [a_1(x), a_2(x), \dots, a_N(x)]$ and $b(x) = [b_1(x), b_2(x), \dots, b_N(x)]$.

The integral terms in (81) yield the system

$$\begin{cases} K_z [A_z(x)a'(x) + B_z(x)b'(x)] = 0 \\ M_z [B_z(x)a'(x) + A_z(x)b'(x)] = -\frac{y(x)}{z+\alpha} \mathbf{1} \end{cases} \quad (83)$$

for all $x \in \overline{\Omega}$, where $\mathbf{1} \in \mathbb{R}^N$ is the vector with one at each entry,

$$[K_z]_{j,i} := \frac{k_j(z)}{k_j(z)^2 - \rho_i(z)^2}, \quad [M_z]_{j,i} := \frac{\rho_i(z)}{k_j(z)^2 - \rho_i(z)^2} \quad (84)$$

and

$$\begin{aligned} A_z(x) &:= \begin{bmatrix} \cosh(\rho_1(z)x) & & 0 \\ & \ddots & \\ 0 & & \cosh(\rho_N(z)x) \end{bmatrix}, \\ B_z(x) &:= \begin{bmatrix} \sinh(\rho_1(z)x) & & 0 \\ & \ddots & \\ 0 & & \sinh(\rho_N(z)x) \end{bmatrix}. \end{aligned} \quad (85)$$

Lemma 13. Suppose that $z \notin \mathcal{S}$ and the characteristic polynomial \mathcal{P}_z has $2N$ distinct roots $\pm\rho_1(z), \dots, \pm\rho_N(z)$. Then the matrices K_z and M_z as defined in (84) are invertible.

Proof. For readability, the dependence on z is omitted in this proof. First, define the Cauchy matrix $C \in \mathbb{C}^{N \times N}$ by

$$C_{j,i} := \frac{1}{n_j - m_i}, \quad n_i := k_i^2, \quad m_i := \rho_i^2, \quad i = 1, \dots, N \quad (86)$$

C is invertible since:

- All n_i are distinct: by definition $z \notin \mathcal{S}$ yields $n_i = k_i^2 \neq k_j^2 = n_j \quad \forall i \neq j$.
- All m_i are distinct: since $\rho_i \neq \rho_j$ for $i \neq j$, the $2N$ distinct roots correspond with N distinct values for m_i .
- $n_j - m_i$ never vanishes: from Proposition 8 follows that $k_j \neq \pm\rho_i$ for all $i, j = 1, \dots, N$, and, by squaring both sides this gives $n_j \neq m_i \quad \forall i, j = 1, \dots, N$.

There holds

$$K_{j,i} = k_j C_{j,i}, \quad M_{j,i} = \rho_i C_{j,i} \quad (87)$$

and therefore

$$|K| = |C| \prod_{i=1}^N k_i, \quad |M| = |C| \prod_{i=1}^N \rho_i. \quad (88)$$

From Proposition 7 follows that $k_i \neq 0$ for all i . The $2N$ roots $\pm\rho_i$ for $i = 1, \dots, N$ of the characteristic polynomial \mathcal{P} are all distinct, thus $\rho_i \neq 0$ for all i . Since C is shown to be invertible, one concludes that $|K| \neq 0$, $|M| \neq 0$ and, hence, K and M are invertible. \square

From the first equation in (83) and Lemma 13 follows that

$$A_z(x)a'(x) = -B_z(x)b'(x) \quad \forall x \in \overline{\Omega}. \quad (89)$$

Multiplying the second equation in (83) with $A_z(x)M_z^{-1}$ and using the identity $A_z(x)^2 - B_z(x)^2 = I$ then yields

$$\begin{aligned} a(x) &= a_{0,z} + \frac{1}{z+\alpha} \int_0^x y(r)B_z(r) dr M_z^{-1} \mathbf{1} \\ b(x) &= b_{0,z} - \frac{1}{z+\alpha} \int_0^x y(r)A_z(r) dr M_z^{-1} \mathbf{1}. \end{aligned} \quad (90)$$

Now, suppose that $y \in Y$ is even. In this case $b_i \in Y$ is odd for all $i = 1, \dots, N$, so $b(0) = 0$ and it obviously follows that $b_{0,z} = 0$. Boundary condition (82) then determines $a_{0,z} \in \mathbb{C}^N$

$$a_{0,z} = (S_z^e)^{-1} \beta_z(y) \quad (91)$$

where

$$\beta_z(y) := -\frac{1}{z+\alpha} \int_0^1 y(r) [S_z^e B_z(r) - S_z^o A_z(r)] dr M_z^{-1} \mathbf{1}. \quad (92)$$

Similarly, for $y \in Y$ odd there holds $a_{0,z} = 0$ and

$$b_{0,z} = (S_z^o)^{-1} \beta_z(y). \quad (93)$$

From now on, suppose that λ is a simple eigenvalue of A and the eigenfunction corresponding to λ is even so that λ is a simple root of $\det(S_\lambda^e)$. Therefore this eigenfunction is of the form $\psi = \{\theta \mapsto e^{\theta\lambda} q_\lambda\}$ with

$$q_\lambda(x) = \sum_{i=1}^N g_i \cosh(\rho_i(\lambda)x) \quad (94)$$

and $g \in \mathbb{C}^N$ a non-trivial solution of $S_\lambda^e g = 0$. It follows that

$$\begin{aligned} (\Delta(z)^{-1}y)(x) &= \frac{y(x)}{z+\alpha} + \sum_{i=1}^N \left[a_i(x) \cosh(\rho_i(z)x) \right. \\ &\quad \left. + b_i(x) \sinh(\rho_i(z)x) \right] \end{aligned} \quad (95)$$

where $a(x), b(x)$ are given by (90). Because y is even, there holds $b_{0,z} = 0$ and $a_{0,z} = (S_z^e)^{-1} \beta_z(y)$.

Eigenvalues in the point spectrum are isolated such that the radius of C_λ can be chosen such that $C_\lambda \cap \sigma(A) = \lambda$. Since M_z^{-1} exists by Lemma 13, all components except the constants of integration $a_{0,z}$ are analytic on C_λ for $x \in \overline{\Omega}$ when $z \notin \mathcal{S}$ and \mathcal{P}_z has $2N$ distinct roots $\forall z \in C_\lambda$. Exploiting this analyticity simplifies (78)

$$\begin{aligned} \frac{1}{2\pi i} \sum_{i=1}^N \cosh(\rho_i(\lambda)x) \oint_{\partial C_\lambda} [a_{0,z}^e]_i dz \\ = v \sum_{i=1}^N g_i \cosh(\rho_i(\lambda)x). \end{aligned} \quad (96)$$

Since (96) holds for all $x \in \overline{\Omega}$, we substitute (91) and obtain

$$\frac{1}{2\pi i} \oint_{\partial C_\lambda} (S_z^e)^{-1} dz \beta_\lambda(y) = v g. \quad (97)$$

Because the inverse is analytic and $\det(S_z^e)$ has a simple root at $z = \lambda$, the residue formula gives

$$\begin{aligned} \frac{1}{2\pi i} \oint_{\partial C_\lambda} (S_z^e)^{-1} dz &= \text{Res} \left(\frac{\text{adj}(S_z^e)}{\det(S_z^e)}, \lambda \right) \\ &= \frac{\text{adj}(S_\lambda^e)}{\frac{d}{dz} [\det(S_z^e)]_{z=\lambda}} \end{aligned} \quad (98)$$

where $\text{adj}(S_z^e)$ denotes the adjugate of S_z^e .

Clearly, the same procedure can be followed if the eigenvalue λ is of the 'odd'-type, i.e. $\det(S_\lambda^o) = 0$.

4.4. Example continued: actual normal form coefficients

In these examples, the characteristic polynomial \mathcal{P} is second order in ρ^2 , so it is straightforward to compute $\rho_1(z)$ and $\rho_2(z)$. We can now construct S_z^e and S_z^o and their adjugates given by (45) and determine

$$\frac{d}{dz} [\det(S_z^e)]_{z=\lambda_i}, \quad \frac{d}{dz} [\det(S_z^o)]_{z=\lambda_i} \quad \text{for } i = 1, 2.$$

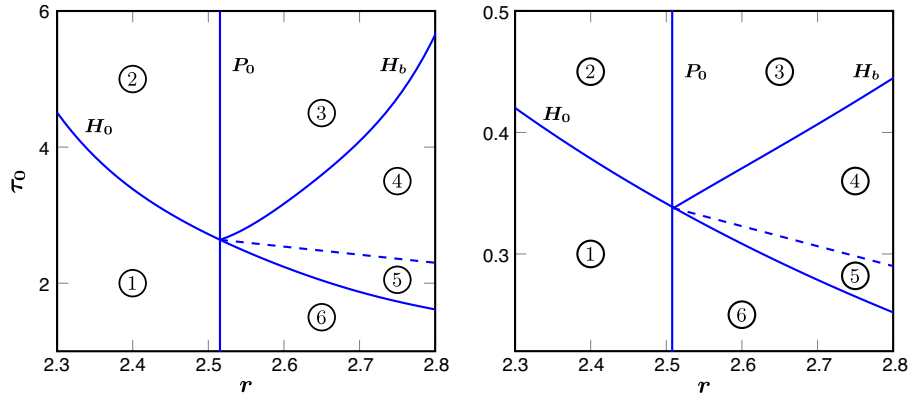


Fig. 7. Bifurcation curves for the discretized system ($m = 100$). H_0 corresponds to a Hopf and P_0 to a pitchfork bifurcation of the background state. H_b corresponds to a Hopf bifurcation of a bump solution. The different parameter regions are numbered corresponding to Fig. 6.

Using Proposition 1 and the eigenfunctions we computed in Section 3 we can now use a symbolic computation package like Maple to determine explicit expressions for y_{kl} , $k, l \in \{1, 2\}$ given by (73). This enables us to compute $\beta_{\lambda_k}(y_{kl})$ given by (92). Finally, we can use (97) and (98) to determine ν .

For the κ_1 -pitchfork–Hopf bifurcation this leads to

$$\begin{bmatrix} p_{11} & p_{12} \\ p_{21} & p_{22} \end{bmatrix} = \begin{bmatrix} g_{300} & g_{111} \\ \text{Re } g_{210} & \text{Re } g_{021} \end{bmatrix} \approx \begin{bmatrix} -0.4074 & -0.6695 \\ -0.8541 & -0.3651 \end{bmatrix}. \quad (99)$$

Since there holds $p_{11}p_{22} > 0$, $b = \frac{p_{12}}{p_{22}} \approx 1.83$, $c = \frac{p_{21}}{p_{11}} \approx 2.10$ and therefore $bc > 1$, we conclude that we are in case Ib.

For the κ_2 -pitchfork–Hopf bifurcation we arrive at

$$\begin{bmatrix} p_{11} & p_{12} \\ p_{21} & p_{22} \end{bmatrix} = \begin{bmatrix} g_{300} & g_{111} \\ \text{Re } g_{210} & \text{Re } g_{021} \end{bmatrix} \approx \begin{bmatrix} -1.8049 & -1.2699 \\ -4.6154 & -0.7859 \end{bmatrix} \quad (100)$$

which also is case Ib with $b \approx 1.62$ and $c \approx 2.56$.

5. Numerical simulation

5.1. Discretization

We can obtain an approximate solution of the delayed neural field equation (26) by discretizing the spatial domain Ω . This leads to a system of equations with $m + 1$ fixed delays and reduces the state space from $C([-h, 0], Y)$ to $C([-h, 0], \mathbb{R}^{m+1})$ for some $m \in \mathbb{N}$. This procedure is described in detail in [26] and a few minor corrections are given in [21].

In our case, the spatial domain $\bar{\Omega} = [-1, 1]$ is discretized into m subintervals of equal length $h = \frac{2}{m}$, leading to

$$\begin{aligned} \frac{dV_i}{dt}(t) &= -\alpha V_i(t) + h \sum_{j=1}^{m+1} a_j \hat{j} (|i-j|h) \\ &\quad \times S(V_j(t - \tau_0 - |i-j|h)) \end{aligned} \quad (101)$$

for $i = 1, \dots, m + 1$ and

$$a_j = \begin{cases} \frac{1}{2} & \text{if } j \in \{1, m+1\} \\ 1 & \text{otherwise} \end{cases}$$

and $\hat{j} : \mathbb{R} \rightarrow \mathbb{R}$ given by (28).

The discretization (101) is a ‘classical’ DDE that can be solved with dde23, a function written in MATLAB. The spectrum of the

discretized system can be determined with DDE-Biftool [31], a numerical bifurcation package for MATLAB. In all examples in this paper, a discretization of $m = 100$ subintervals is used.

5.2. Example continued: bifurcation analysis and simulation results

With the help of DDE-Biftool we can determine the Hopf bifurcation curves of the non-trivial stationary solutions born at the pitchfork bifurcations of the background state in the discretized system. The borders of the bistable regions are estimated by numerical simulations. We also compute the pitchfork and Hopf bifurcation curves of the background state in the discretized system.

We now present simulations of the system in the six parameter regions in Fig. 7 for both connectivities and initial conditions

$$V(x, t) = 0.05 (0.99x + 0.01) \quad (102a)$$

$$V(x, t) = 0.05 (0.01x + 0.99) \quad (102b)$$

respectively

$$V(x, t) = 0.05 (0.7 \cos(4.30x) + 0.3 \cos(2.04x)) \quad (103a)$$

$$V(x, t) = 0.05 \quad (103b)$$

for $t \in [-(\tau_0 + 2), 0]$.

In region 1 the background state is globally stable and, indeed, all solutions decay to zero in Fig. 8.

In region 2 the background state has lost its stability due to a Hopf bifurcation and a stable periodic solution has emerged, as is clearly visible in Fig. 9. Due to the fact that the initial conditions (102a) and (103a) are located close to the stable manifolds of the background state we observe a longer transient.

Moving from region 2 to region 3 corresponds to crossing the pitchfork curve P_0 in Fig. 7. The oscillation around the background state remains the only stable solution. Now, however, an unstable stationary solution also exists. Since initial conditions (102a) and (102b) lie close to the stable manifolds of these unstable equilibria, they are clearly visible in the transient in Fig. 10.

The most interesting region is region 4, since it is characterized by bistability, i.e. the coexistence of a periodic and a stationary solution. Simulations in this region are shown in Fig. 11.

Simulations in regions 5 and 6 are shown in Figs. 12 and 13. They correspond to regions 3 and 2 respectively, where the role of the stationary and the periodic solution is interchanged.

6. Discussion

By extensively studying two particular pitchfork–Hopf bifurcations we have shown how spectral properties can be analyzed

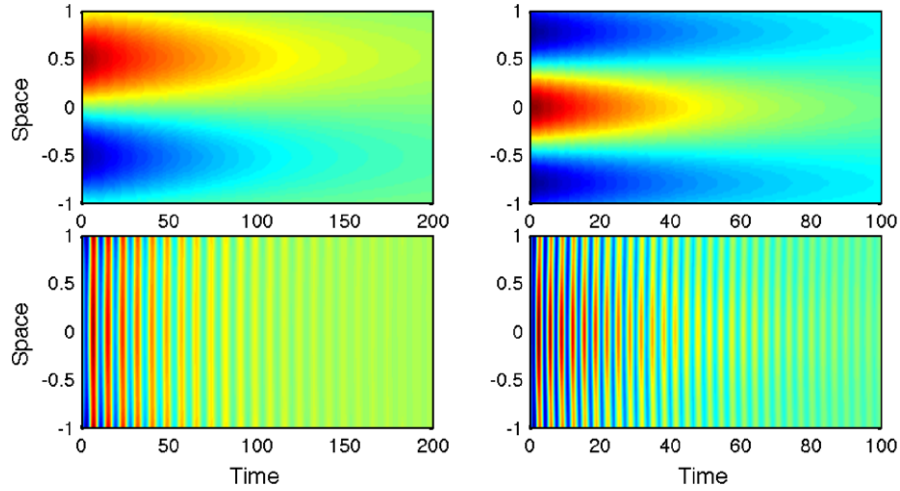


Fig. 8. Simulations in region 1. *Left* panel corresponds to connectivity \hat{j}_1 with $r = 2.4$ and $\tau_0 = 0.3$, *right* panel to connectivity \hat{j}_2 with $r = 2.4$ and $\tau_0 = 2.2$. *Top* and *bottom* correspond to initial conditions (102a), (103a) and (102b), (103b) respectively.

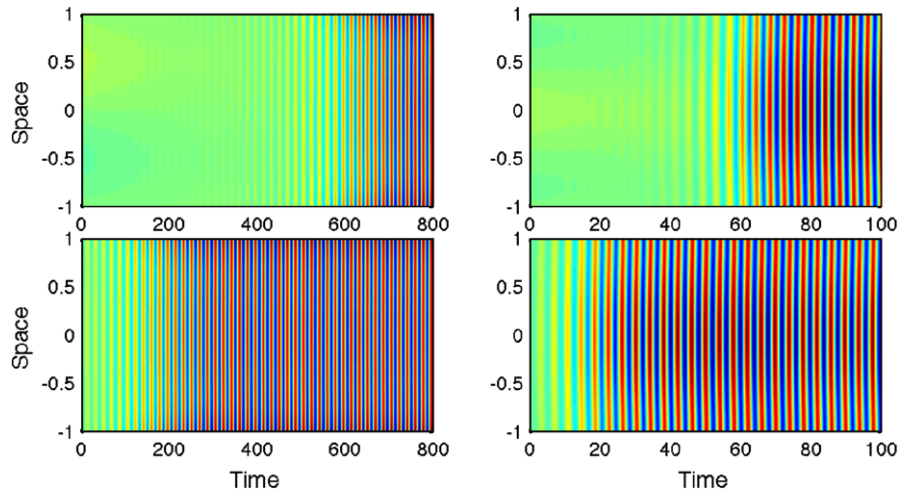


Fig. 9. Simulations in region 2. *Left* panel corresponds to connectivity \hat{j}_1 with $r = 2.4$ and $\tau_0 = 0.6$, *right* panel to connectivity \hat{j}_2 with $r = 7$ and $\tau_0 = 2.2$. *Top* and *bottom* correspond to initial conditions (102a), (103a) and (102b), (103b) respectively.

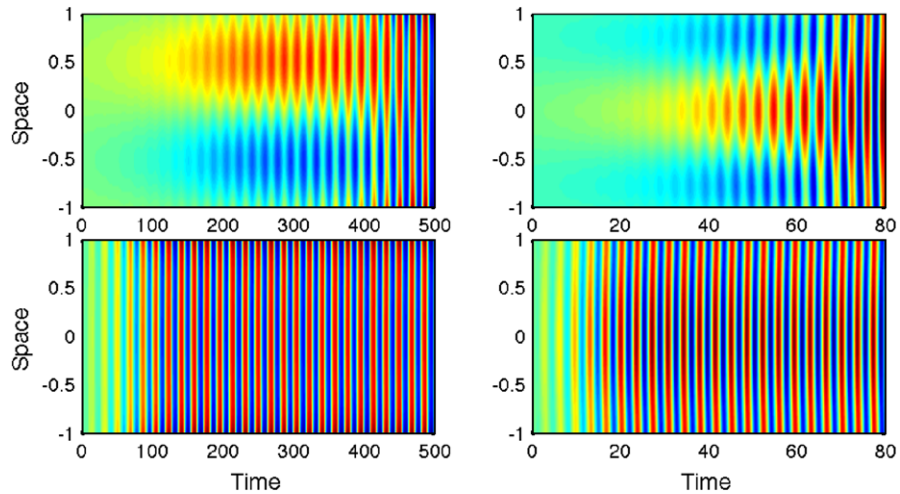


Fig. 10. Simulations in region 3. *Left* panel corresponds to connectivity \hat{j}_1 with $r = 2.8$ and $\tau_0 = 0.45$, *right* panel to connectivity \hat{j}_2 with $r = 2.8$ and $\tau_0 = 7$. *Top* and *bottom* correspond to initial conditions (102a), (103a) and (102b), (103b) respectively.

and normal form coefficients can be evaluated for a special type of (scalar and one-dimensional) delayed neural field equations. Our specific choice of an odd firing rate function greatly simplifies the

computation of the normal form coefficients. While being mathematically very convenient, there is no biological reason why the firing rate function should necessarily possess this kind of symmetry.

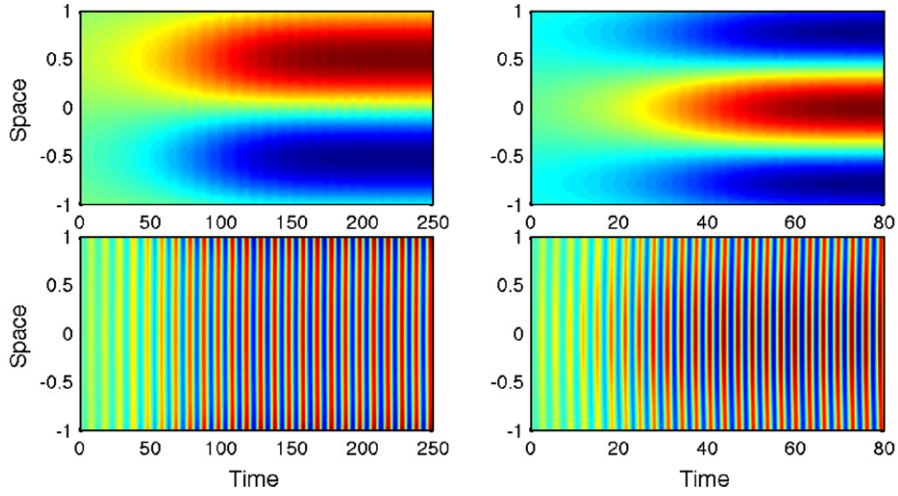


Fig. 11. Simulations in region 4. *Left* panel corresponds to connectivity \hat{j}_1 with $r = 2.4$ and $\tau_0 = 0.32$, *right* panel to connectivity \hat{j}_2 with $r = 2.8$ and $\tau_0 = 3$. *Top* and *bottom* correspond to initial conditions (102a), (103a) and (102b), (103b) respectively.

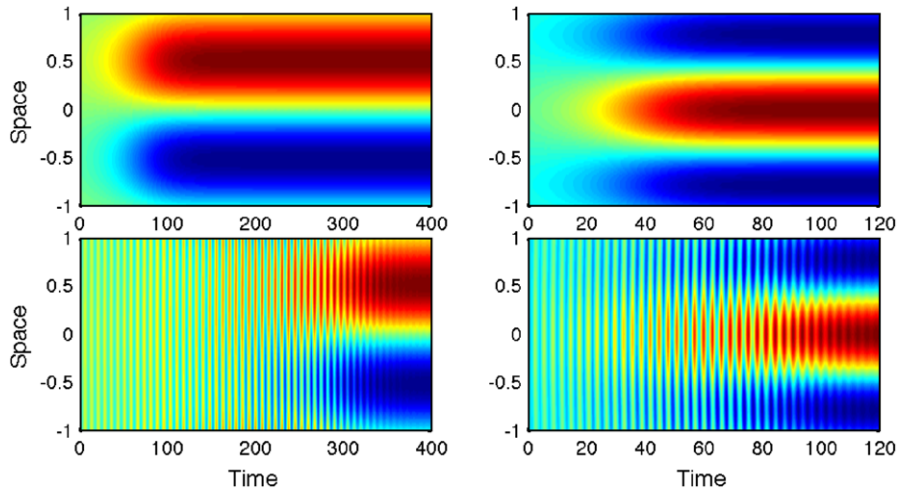


Fig. 12. Simulations in region 5. *Left* panel corresponds to connectivity \hat{j}_1 with $r = 2.8$ and $\tau_0 = 0.26$, *right* panel to connectivity \hat{j}_2 with $r = 2.8$ and $\tau_0 = 1.8$. *Top* and *bottom* correspond to initial conditions (102a), (103a) and (102b), (103b) respectively.

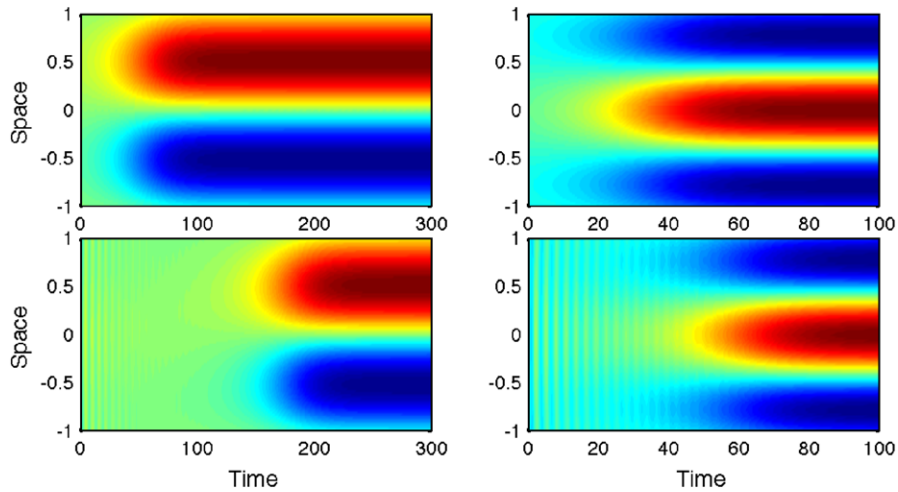


Fig. 13. Simulations in region 6. *Left* panel corresponds to connectivity \hat{j}_1 with $r = 2.8$ and $\tau_0 = 0.18$, *right* panel to connectivity \hat{j}_2 with $r = 2.8$ and $\tau_0 = 1$. *Top* and *bottom* correspond to initial conditions (102a), (103a) and (102b), (103b) respectively.

Luckily however, the techniques presented in Section 4.3 are still applicable for much more general forms of the firing rate function, but make the resulting formulas more involved.

In our particular examples we chose so called ‘Wizard-hat’ connectivity function (see Fig. 1), which models a mixed population of interacting inhibitory and excitatory neurons with local excitation

and distal inhibition and goes back to Amari [10]. This type of connectivity is used in models of orientation tuning in the visual cortex (see e.g. [32]) and in models of short term working memory (see e.g. [33]). At first sight this type of connectivity seems to disagree with experimental data, since there is a consensus that long-range connections between neurons are excitatory. However, although long-range *connections* are excitatory, long-range *interactions* can be inhibitory [34].

By evaluating the normal coefficients we predicted a region in parameter space where a stable stationary and a stable periodic solution coexist and confirmed this by numerical simulations (see Fig. 11). Multistability in neural field models is always very interesting since it implies that a short external input (in the form of an additional input term $I(\mathbf{r}, t)$ in the right hand side of (NFE)) can lead to a drastic and permanent change in dynamics. In our particular case, we can for example switch from a stable stationary state to a large-scale oscillation, a regime which could be linked to an epileptic seizure [35].

Other possible dynamics at a pitchfork–Hopf bifurcation include stable oscillations around a non-trivial steady state in the ‘simple cases’ and tori in the ‘difficult’ cases. However, we were not able to find these in our particular model.

Neural fields model the behavior of large networks of neurons and, to arrive at a formulation as concise as (NFE), a lot of approximations and simplifications have to be made. Therefore, certain situations may arise in which one has to augment the neural field equations with additional variables. It is for example known that ion homeostasis breaks down in certain pathological brain states and, in this case, it may be necessary to explicitly model extracellular space. It is one of the many challenging future tasks in theoretical neuroscience to develop models which are precise enough to capture all relevant dynamics but concise enough to be analytically traceable.

References

- [1] W. van Drongelen, H.C. Lee, M. Hereld, D. Jones, M. Cohoon, F. Elsen, M.E. Papka, R.L. Stevens, Simulation of neocortical epileptiform activity using parallel computing, *Neurocomputing* 58–60 (2004) 1203–1209.
- [2] W. van Drongelen, H.C. Lee, H. Koch, F. Elsen, M.S. Carroll, M. Hereld, R.L. Stevens, Interaction between cellular voltage-sensitive conductance and network parameters in a model of neocortex can generate epileptiform bursting, in: Annual International Conference of the IEEE Engineering in Medicine and Biology—Proceedings, 2004, pp. 4003–4005.
- [3] E.M. Izhikevich, Simple model of spiking neurons, *IEEE Trans. Neural Netw.* 14 (2003) 1569–1572.
- [4] N.F. Rulkov, Modeling of spiking–bursting neural behavior using two-dimensional map, *Phys. Rev. E* 65 (2002) 041922.
- [5] N.F. Rulkov, I. Timofeev, M. Bazhenov, Oscillations in large-scale cortical networks: map-based model, *J. Comput. Neurosci.* 17 (2004) 203–223.
- [6] R.W. Williams, K. Herrup, The control of neuron number, *Annu. Rev. Neurosci.* 11 (1988) 423–453.
- [7] H.R. Wilson, J.D. Cowan, Excitatory and inhibitory interactions in localized populations of model neurons, *Biophys. J.* 12 (1972) 1–24.
- [8] H.R. Wilson, J.D. Cowan, A mathematical theory of the functional dynamics of cortical and thalamic nervous tissue, *Kybernetik* 13 (1973) 55–80.
- [9] S. Amari, Homogeneous nets of neuron-like elements, *Biol. Cybernet.* 17 (4) (1975) 211–220.
- [10] S. Amari, Dynamics of pattern formation in lateral-inhibition type neural fields, *Biol. Cybernet.* 27 (2) (1977) 77–87.
- [11] P.L. Nunez, The brain wave equation: a model for the EEG, *Math. Biosci.* 21 (3–4) (1974) 279–297.
- [12] S. Coombes, C. Laing, Delays in activity-based neural networks, *Philos. Trans. R. Soc. Lond. Ser. A Math. Phys. Eng. Sci.* 367 (1891) (2009) 1117–1129.
- [13] A. Hutt, Local excitation–lateral inhibition interaction yields oscillatory instabilities in nonlocally interacting systems involving finite propagation delays, *Phys. Lett. A* 372 (2008) 541–546.
- [14] A. Hutt, F.M. Atay, Effects of distributed transmission speeds on propagating activity in neural populations, *Phys. Rev. E* (3) 73 (2) (2006) 021906, 1–5.
- [15] A. Hutt, F.M. Atay, Spontaneous and evoked activity in extended neural populations with gamma-distributed spatial interactions and transmission delay, *Chaos Solitons Fractals* 32 (2) (2007) 547–560.
- [16] A. Roxin, E. Montbrío, How effective delays shape oscillatory dynamics in neuronal networks, *Physica D* 240 (3) (2011) 323–345.
- [17] N.A. Venkov, S. Coombes, P.C. Matthews, Dynamic instabilities in scalar neural field equations with space-dependent delays, *Physica D* 232 (1) (2007) 1–15.
- [18] S. Visser, H.G.E. Meijer, M.J.A.M. van Putten, S.A. van Gils, Analysis of stability and bifurcations of fixed points and periodic solutions of a lumped model of neocortex with two delays, *J. Math. Neurosci.* 2 (1) (2012) 1–30.
- [19] L. Zhang, How do synaptic coupling and spatial temporal delay influence traveling waves in nonlinear nonlocal neuronal networks? *SIAM J. Appl. Dyn. Syst.* 6 (3) (2007) 597–644.
- [20] S.A. Campbell, Time delays in neural systems, in: *Handbook of Brain Connectivity*, Springer, Berlin, 2007, pp. 65–90.
- [21] S.A. van Gils, S.G. Janssens, Yu.A. Kuznetsov, S. Visser, On local bifurcations in neural field models with transmission delays, *J. Math. Biol.* 66 (4–5) (2013) 837–887.
- [22] R. Veltz, Interplay between synaptic delays and propagation delays in neural field equations, *SIAM J. Appl. Dyn. Syst.* 12 (3) (2013) 1566–1612.
- [23] O. Diekmann, S.A. van Gils, S.M. Verduyn Lunel, H.-O. Walthers, *Delay Equations: Functional, Complex, and Nonlinear Analysis*, in: *Applied Mathematical Sciences*, vol. 110, Springer-Verlag, New York, 1995.
- [24] G. Greiner, J.M.A.M. van Neerven, Adjoints of semigroups acting on vector-valued function spaces, *Israel J. Math.* 77 (3) (1992) 305–333.
- [25] K.-J. Engel, R. Nagel, *One-Parameter Semigroups for Linear Evolution Equations*, in: *Graduate Texts in Mathematics*, vol. 194, Springer, New York, 2000.
- [26] G. Faye, O. Faugeras, Some theoretical and numerical results for delayed neural field equations, *Physica D* 239 (9) (2010) 561–578.
- [27] A. Vanderbauwhede, Local Bifurcation and Symmetry, in: *Research Notes in Mathematics*, vol. 75, Pitman, Boston, MA, 1982.
- [28] Yu.A. Kuznetsov, *Elements of Applied Bifurcation Theory*, third ed., in: *Applied Mathematical Sciences*, vol. 112, Springer, New York, 2004.
- [29] R. Veltz, O. Faugeras, A center manifold result for delayed neural fields equations, *SIAM J. Math. Anal.* 45 (3) (2013) 1527–1562.
- [30] J. Guckenheimer, P. Holmes, *Nonlinear Oscillations, Dynamical Systems, and Bifurcations of Vector Fields*, in: *Applied Mathematical Sciences*, vol. 42, Springer, New York, 1983.
- [31] K. Engelborghs, T. Luzyanina, D. Roose, Numerical bifurcation analysis of delay differential equations using DDE-BIFTOOL, *ACM Trans. Math. Software* 28 (2002) 1–21.
- [32] R. Ben-Yishai, R.L. Bar-Or, H. Sompolinsky, Theory of orientation tuning in visual cortex, *Proc. Natl. Acad. Sci. USA* 92 (9) (1995) 3844–3848.
- [33] C.R. Laing, W.C. Troy, Two-bump solutions of Amari-type models of neuronal pattern formation, *Physica D* 178 (3–4) (2003) 190–218.
- [34] K. Kang, M. Shelley, H. Sompolinsky, Mexican hats and pinwheels in visual cortex, *Proc. Natl. Acad. Sci. USA* 100 (5) (2003) 2848–2853.
- [35] F. Lopes Da Silva, W. Blanes, S.N. Kalitzin, J. Parra, P. Suffczynski, D.N. Velis, Epilepsies as dynamical diseases of brain systems: basic models of the transition between normal and epileptic activity, *Epilepsia* 44 (12 Suppl.) (2003) 72–83.